SAND2019-14336C

Soot Concentration, Temperature, and Radiant Emission Measurements in a Turbulent Ethylene Jet Flame

Christopher R. Shaddix, Jiayao Zhang*, and Timothy C. Williams†

Combustion Research Facility
Sandia National Laboratories
Livermore, California 94550

Abstract

This work reports on a combined set of measurements of soot concentration, soot temperature, and radiant emission in a turbulent ethylene non-premixed jet flame with a jet exit Reynolds number of 20,000. The soot concentration measurements were measured via trapping-corrected laser-induced incandescence (LII) and validated via full-flame extinction. Soot temperature was measured simultaneously with soot concentration via an extinction/emission diagnostic with a local probe volume determined by two thin refractory probes. Radiant emission was quantified with a custom-built narrow-angle radiometer. The soot concentrations peak at a mean value of 0.6 ppm at mid-height of this flame. Mean soot temperatures are in the vicinity of 1550 K through the middle of the flame and then drop off near the top of the flame. Higher mean soot temperatures are found over the lower portion of the flame, reaching 1600 K along the centerline and 1730 K in the annulus. Evaluation of simultaneous OH PLIF/soot LII images taken in this flame explains these trends in soot temperature. The mean radiant emission peaks at 17.5 kW/m2-sr, at nearly the same height as the peak of the mean soot volume fraction. This combined set of carefully measured and analyzed data from a burner designed for

---

* Present address: Apple Inc., Cupertino, CA 95014

† Present address: T.C. Williams and Associates, Livermore, CA 94550.

comparison with modeling results is a useful target for numerical predictions of turbulent sooty flames with a significant soot concentration.

Keywords: turbulent flame; soot; radiation; temperature; ethylene

1. Introduction

The health effects of fine particulate matter (PM2.5) in ambient air have become increasingly evident over the past two decades. These particles deeply penetrate lung tissue and have been shown to affect the pulmonary and cardiovascular systems, leading to increased morbidity and mortality [1]. There have been many studies attempting to differentiate health effects from different components of PM2.5, with mixed success. It is clear, however, that soot particles (elemental carbon) contribute to the health impacts of PM2.5 [2-4]. Because of this association between soot particles in the atmosphere and deleterious health, soot emissions from combustion sources have faced increasingly stringent regulation. Furthermore, atmospheric soot has been shown to enhance climate forcing [5], and in-flight emission of soot from aircraft engines has been shown to influence contrail/cloud formation [6].

Despite decades of efforts, the combustion R&D community still lacks a truly predictive modeling capability for soot formation and emission in turbulent flames, which are present in internal combustion engines, gas turbines, and furnaces. Soot formation has proven to be an exceptionally difficult phenomenon to effectively model because of the complexity of the chemical reactions that are involved and their relatively long temporal duration, making soot formation very sensitive to local flame strain and differential diffusion, and their temporal dynamics. Beyond the complexity of the processes involved, another reason for the lack of predictive models is the lack of robust, spatially and temporally resolved data in sooting turbulent flames. Such datasets have been in development for many years for soot-free flames [7] and more recently for a slightly sooting methane flame [8], but available

experimental datasets for moderate sooting turbulent flames are largely lacking. Such datasets are needed because under moderately sooting flame conditions, the soot that is formed radiates energy away from the hottest soot-containing regions to the walls of enclosures and to the cooler soot-containing regions of the flame, thus redistributing the reaction enthalpy and influencing the flame chemistry and burning rate in a coupled manner [9]. The ability of computational models to accurately describe these coupled soot formation/radiation/flame chemistry interactions cannot be evaluated with data from soot-free or even lightly sooting flames.

Previously, we have reported on the design of piloted, turbulent non-premixed jet flame burners for using higher hydrocarbon fuels, specifically on two designs for studying ethylene flames and flames fueled by prevaporized aviation fuel [10]. In this paper we present results from the use of several spatially and temporally resolved diagnostics on soot concentrations, radiant emission, and joint soot concentration-temperature data in a non-premixed ethylene jet flame with a fuel exit Reynolds number of 20,000. The soot temperature measurements, together with joint imaging of soot and OH, reveal a previously unreported phenomenon in these moderately sooty flames – elevated soot temperatures lower in the flame, where soot forms adjacent to the high temperature flame sheet.

2. Experimental Methods

2.1 Turbulent non-premixed ethylene flame

Measurements were performed in a piloted turbulent non-premixed ethylene jet flame stabilized on a burner designed along the same principle as the well-known Sydney burner [11]. The burner has a central fuel tube with a 3.35 mm ID and a concentric outer tube with a 19.1 mm OD. A pilot plate is situated in the annulus between the two tubes, recessed from the lip, and contains three concentric rows of equally distributed holes, supporting tiny flames for stabilizing the primary jet flame. While the central jet was composed of pure ethylene, a premixed ethylene/air mixture at an equivalence ratio of 0.9

was supplied to the pilot holes at a flow rate corresponding to 2% of the energy release rate of the main jet. With this design, the jet flames showed good flame attachment, even for fuel jet Reynolds numbers (Re) exceeding 30,000. The burner was positioned on top of a vertical wind tunnel that provided co-flowing dry air at 0.6 m/s, to prevent room-air disturbance and provide well-established boundary conditions for flame modeling. The whole assembly was mounted on a platform with XYZ translation to easily change the flame measurement location.

A flame with a fuel jet Reynolds number of 20,000 (corresponding to a fuel mass flow rate of 26.4 slpm at 298 K) was investigated in this study. This flame has sufficiently strong turbulence to minimize the influence of buoyancy and to test the robustness of combustion models but avoids frequent local flame extinction events in the high-shear region just above the burner lip (as verified with OH PLIF imaging [10]). Jet flames with flame extinction and subsequent reignition pose a major challenge for flame modeling [12], even in the absence of soot and its associated radiant heat transfer. For the broadest applicability to near-term turbulent flame modeling, it seemed prudent to perform measurements in a flame without significant local extinction. The heat release rate of the flame was 24.0 kW and it had a visible flame height of approximately 870 mm.

2.2 Laser-induced incandescence and laser extinction measurements

Soot concentration was determined using LII, as excited by the fundamental infrared (IR) output of a Nd:YAG laser (1064 nm) that was expanded into a sheet using a concave cylindrical lens (focal length of –75 mm) and a convex spherical lens (focal length of 1000 mm). The use of IR excitation instead of the commonly used 532 nm excitation offers the advantages of substantially reduced photochemical interference from other species, such as C_2 or C_3 [13,14], as well as significantly reduced laser extinction across the flame. Further, with IR laser excitation a wide band of visible wavelengths can be used to capture the LII signal, reducing its sensitivity to signal trapping. The thickness of the laser sheet, defined as the $1/e^2$ width, was found to be 275 μm, with a variation of less than 15% across the field-of-

view of the imaging camera. A laser pulse energy of 66 mJ was used, giving a fluence of 0.6 J/cm^2. The LII fluence response was found to give a nominally flat 'plateau' from 0.3 to 0.7 J/cm^2, as shown in Fig. 1. Therefore, the LII signal was nearly independent of shot-to-shot fluctuations in the laser power or attenuation of the laser sheet as it passed through the sooty flame.

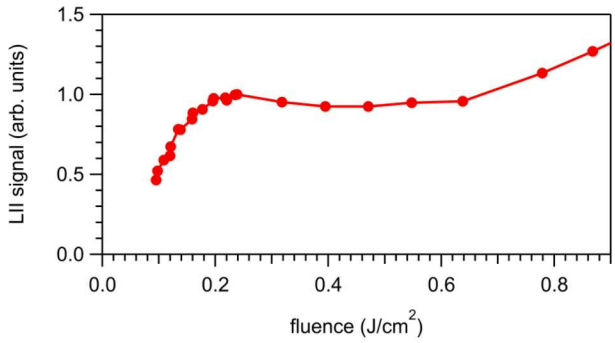

Figure 1: Measured fluence dependence of LII signals generated from a Gaussian laser sheet.

The LII signals were collected by a Princeton Instruments intensified, fast-gating CCD camera mounted perpendicular to the laser path. The camera has a full-frame 512×512 CCD array and was set to image an area of 60×60 mm^2 (117 μm on each pixel). It was equipped with a Nikkor 50-mm focal length f/1.2 lens (Nikon), whose aperture was stepped down to f/2 in order to minimize optical aberrations (primarily coma) in the peripheral region of the FOV of this camera. LII signal was collected through a Schott BG-14 glass filter and a 600-nm short-pass filter, effectively accepting light from 300 to 600 nm. The camera gate was set to 50 ns with zero delay from the laser pulse. 1000 LII images were acquired at each flame height, together with 500 images of the flame with the lasers blocked to provide background correction.

The LII signals were calibrated for soot volume fraction by performing both LII imaging and laser extinction measurements with a cw HeNe laser (632.8 nm) on a laminar ethylene jet flame with a cold flow velocity of 0.41 m/s, anchored on the same jet burner as used for the turbulent flame. The

transmitted laser light was collected in an integrating sphere and then detected on a photodiode after passing through a laser line filter. The soot concentration was deduced from the measured extinction using a dimensionless extinction coefficient, K_e, of 9.3, which is an average of those determined for soot sampled from laminar ethylene diffusion flames by Williams et al. [15] and which also corresponds to a midpoint value of the range of dimensionless extinction coefficients reported for soot emitted from both laminar and turbulent ethylene flames [15].

Once calibrated, the LII measurements were corrected for time-averaged signal trapping at any given position by first symmetrizing the data and then applying an onion-peeling approach previously described in ref. [16]. A soot absorption coefficient (as distinct from the extinction coefficient, particularly for the aggregated soot we expect in most regions of this flame) has been shown to be appropriate when performing signal trapping corrections with laser sheet excitation [17], so a value of K_a of 7.4, as recommended by Bond and Bergstrom [18] and similar to that determined by Williams et al. [15] for ethylene and jet fuel soot, was applied here. A final, semi-independent check of the accuracy of the LII data calibration and signal trapping procedure was performed by making full-flame laser extinction measurements (using the integrating sphere to guard against beam steering losses) and comparing these to the extinction that the corrected LII measurements predict, using the same K_e value as assumed in interpreting the LII calibration in the laminar flame.

2.3 Radiant emission measurements

Radiant emission from the flame was measured with a custom-built radiometer that consisted of a thin-film thermopile detector (Dexter, Type 1M), with a calcium fluoride window that transmits radiation between 0.2 – 8 μm, which covers nearly all of the important radiation from flames. A black-anodized, water-cooled steel tube was attached to the radiometer to restrict the incident radiation to a small solid angle (Ω) of 1.065×10^{-4} sr. The detector sensor was located 500 mm away from the jet axis. During experiments, the burner was traversed axially in 10 mm increments and (at certain heights) radially in 5

mm increments to measure radiation along different paths. 50 repeat records were collected at each measurement location. As the radiative heat exchange and the electronic response of the thermopile detector are affected by its own temperature, care was taken to stabilize the thermal environment of the detector. The radiometer signals were calibrated using a high-temperature blackbody source as a reference. Because of its intrinsic thermal inertia, the thermopile detector has a finite time constant of 12.8 ms, equivalent to employing a low-frequency-pass filter with a 3dB cut-off frequency of 12.4 Hz. Besides the bias resulting from its limited frequency response, the uncertainties in these radiation measurements result primarily from the electronic noise and the detector temperature offset, which amount to approximately 3% uncertainty.

2.4 Joint soot temperature/concentration measurements

Figure 2 shows a schematic of the 3-line diagnostic that was implemented. Laser attenuation was performed with a 632.8 nm HeNe laser, so that soot dimensionless extinction coefficients previously measured at this wavelength could be utilized to interpret the measurement. A reference laser intensity measurement was made using a beamsplitter and a photodiode detector with a 632.8 nm laser line filter (3 nm FWHM). After passing through the flame probe volume, the laser beam was separated from the 2-color soot emission signals with the use of a dichroic beamsplitter. The transmitted beam was collected in a 12-inch diameter integrating sphere, before passing through a laser line filter onto a photodiode detector, to remove any influence from turbulent flame beam steering on the attenuation measurement. The soot emission signals were split with a cube beamsplitter and then passed through bandpass filters with center wavelengths of 850 nm and 1000 nm before passing onto thermoelectrically cooled avalanche photodiode (APD) detectors. Calibration of the two-color pyrometry diagnostic was performed using a high-temperature blackbody source and a mirror that redirected the blackbody light towards the avalanche photodiode detectors.

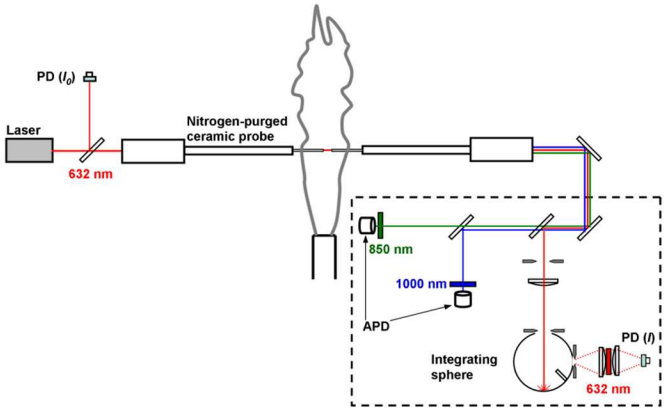

Figure 2: Schematic of diagnostic configuration used to perform 3-line measurements of soot temperature/concentration statistics in the turbulent jet flames.

A key aspect of the 3-line diagnostic technique is the need to insert a two-ended probe into the flame to limit the length of the optical interrogation region. In previous studies, these probes have typically been constructed of water-cooled steel or aluminum tubing, in some cases with insulation wrapped around the outside of the probes. With this design approach, the probe tubes are necessarily quite large and generate a thick thermal quench layer. To minimize probe perturbation of the flow field and flame sheets, we adopted the approach first used by Sivathanu and Faeth [19], with tapered refractory probe ends that are uncooled. The alumina probes had a final OD of 6.35 mm and were found to transmit radiant emission from the broader flame through the walls to the pyrometry detectors at measurable levels. Therefore, the outer surfaces of the probes were painted black with high-temperature paint, which corrected this problem. Furthermore, a small amount of radiation was transmitted to the detectors from the hot tips of the probes when they were located in the hottest regions of the flames, leading to a non-zero radiant background signal. This background signal was subtracted before processing the datasets to determine the soot radiant temperature.

Data were collected along the flame centerline at many different heights and radial traverses were performed at 15 selected heights. A data sampling rate of 5 kHz was used to resolve the turbulent

motion of the soot. Digital time records were collected as 40 sets of 5000 data points (i.e. a 1 sec time record) at a given location in the flame before a computer-controlled X-Y-Z translation stage moved the flame to the next programmed sampling position. A 10 mm probe end separation was used for most of the measurements, but some data were also collected for probe separations of 5 mm and 20 mm. The soot extinction measurement was converted to soot volume fraction with a dimensionless extinction coefficient of 9.3, as described previously. The optical path length of soot extinction was assumed to be equal to 2 mm less than the probe tip separation, to account for the effect of the small purge flow of nitrogen out the tips of the probe.

3. Results and Discussion

3.1 Soot volume fraction

Figure 3 shows planar soot volume fraction image data derived from LII measurements in the ethylene flame, including instantaneous snapshots, the temporal mean, and the root mean square (rms) variations in soot concentration, expressed in terms of parts per million (ppm) by volume. Note that the mean and rms images have not been corrected for signal trapping, as that correction was easier to apply to individual horizontal data profiles. It is apparent from Fig. 3, especially when viewing the rms images, that despite our best efforts to make the LII excitation beam as uniform as possible, there are repeatable variations in the LII signals from top-to-bottom of an image. To correct for this in extracted horizontal line profiles, a consistent vertical position within each image was selected.

It is evident from Fig. 3 that the soot field is highly intermittent in this turbulent flame. The peak values of soot concentration in the instantaneous images are approximately 4 ppm, similar to the maximum soot concentrations (when using the K_e value used here) in laminar ethylene flames, whereas the mean soot concentration peaks at 0.5 ppm. Further evidence of the strong intermittency is shown by the rms values, whose magnitudes are as large as the mean values throughout the primary sooting region of the flame.

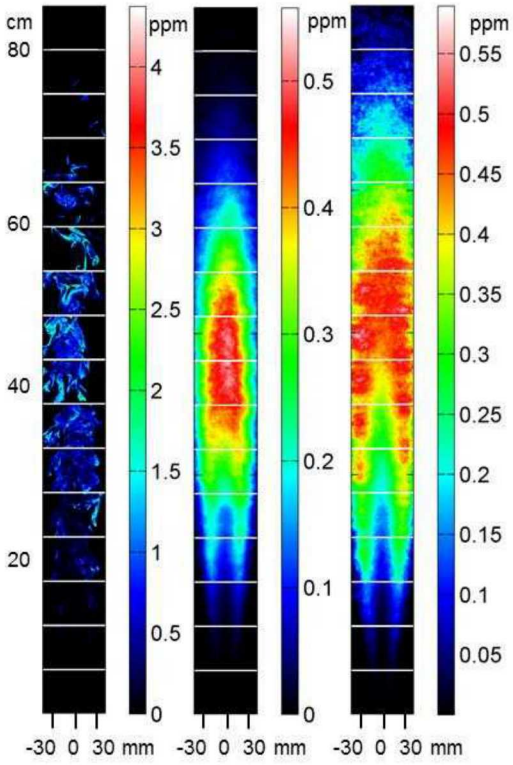

Figure 3: Instantaneous, mean, and rms (left-to-right) of soot volume fractions measured by LII imaging in the ethylene flame. The instantaneous image is a collage of images taken at different heights.

Horizontal profiles of mean soot volume fraction in 50 mm increments of height are shown in Fig. 4. With the signal trapping correction, the peak mean soot volume fraction in this flame is seen to be at 0.6 ppm, at a height of approximately 450 mm. (The signal trapping correction is largest along the centerline and peaks at 16% for the maximum mean soot volume fraction in this flame.) These concentrations compare favorably to those that have been reported for other turbulent ethylene jet flames, once corrections are made for the assumed dimensionless extinction coefficient used to quantify the soot concentration measurements. For example, Coppalle and Joyeaux [20] studied an ethylene jet flame with Re = 11800, supported on a tube of 4 mm diameter and measured a peak time-averaged soot volume fraction of 1.9 ppm, at a height of 380 mm, when using a probe-based laser extinction technique

and an assumed K_e of 3.5. Their peak concentration corresponds to 0.7 ppm when using a K_e of 9.3, as used in the current study. Hu et al. [21] investigated an ethylene flame with Re = 13500 on a 4.5 mm tube diameter and found the peak mean soot volume fraction to be approximately 1.2 ppm, when using probe-based laser extinction and an assumed K_e of 3.7. This corresponds to a value of 0.5 in the context of the current study. Lee et al. [22] investigated ethylene jet flames with Re varying from 4000 to 23000. They found a peak mean soot volume fraction of approximately 1 ppm for flames with Re near 20000, when using an assumed K_e of 4.9 to calibrate their LII measurements. In the context of the current study, the peak mean soot volume fraction corresponds to 0.5 ppm, which is very consistent with the results here, considering that Lee et al. did not employ a signal trapping correction to their LII detection at 400 nm. Lee et al. also found the soot concentration rms to be of similar magnitude to the mean concentration, consistent with the results here.

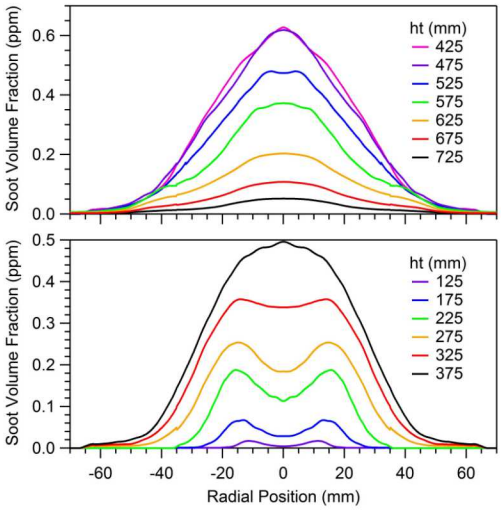

Figure 4: Symmetrized and trapping-corrected soot volume fraction profiles in the ethylene jet flame, at 50 mm intervals of height.

Figure 5 shows the measured full-flame HeNe laser transmittance, together with the calculated transmittance generated from the trapping-corrected LII mean soot volume fractions. The agreement in the two curves is very good, with only some minor deviation in the upper regions of the flame.

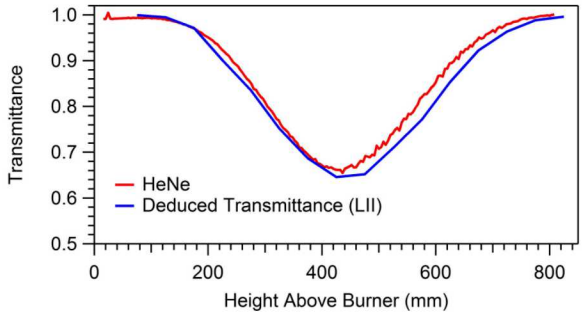

Figure 5. Comparison of measured centerline transmittance of a HeNe laser beam across the jet flame and the 633 nm transmittance deduced from the LII-determined soot volume fraction field, after correction for signal trapping.

3.2 Thermal radiation

Figure 6 shows the mean centerline radiant emission. It is clear from comparing Figs. 5 and 6 that the soot optical thickness (as represented by the full-flame HeNe laser extinction = 1/transmittance) shows the same general profile as the radiant emission from the flame, suggesting a strong contribution of radiation from soot to the overall flame emission. The radiation peaks at a height of 430 mm, essentially at the same height as the peak soot volume fraction. Measured radial profiles are shown in Fig. 7 and show the expected widening of emission profiles with increasing height, continuing into the post-flame region where all of the soot has been oxidized.

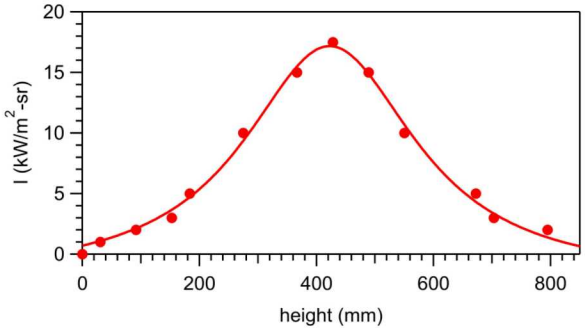

Figure 6: Measured centerline thermal radiant emission, together with a Voigt profile fit to the data.

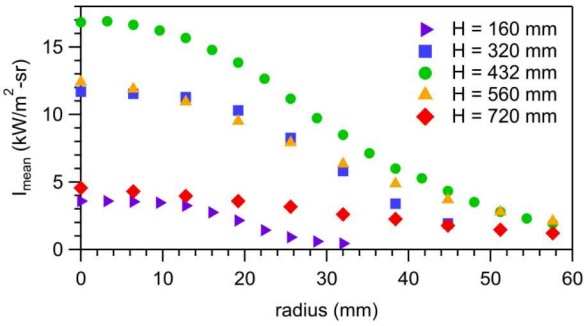

Figure 7: Measured radial profiles of radiant emission at selected heights.

3.3 Soot temperature/concentration

Figure 6 shows the mean soot temperatures in the flame. Somewhat surprisingly, the highest time-average soot temperatures occur low in the flame, shortly after soot has begun to form, and show a strong annular character with cooler soot towards the centerline. Further up, the soot temperature profiles flatten and then ultimately decrease through the oxidation zone. It is important to recall that the 3-line measurement of soot temperature only makes a measurement at those instants when soot is present within the optical probe volume and the only contribution to the measured signal arises from those regions of the probe volume that contain soot at that moment in time. Therefore, it cannot be equated to a general measurement (or modeling prediction) of gas temperature at a given location.

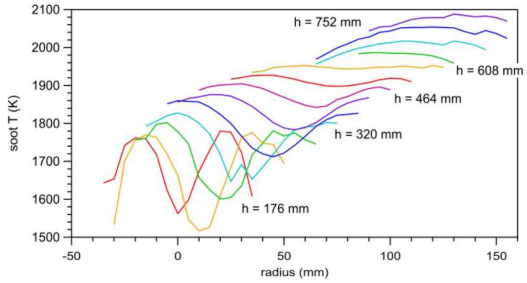

Figure 8: Staggered radial profiles of mean soot temperature. Each profile is staggered from the next lower in height by 50 K in temperature and 10 mm in radial position.

To better understand the cause of the higher soot temperatures low in the flame, the probability density functions of soot temperature and soot volume fraction were computed, as well as the joint

probability distributions. These showed consistently hotter soot low in the flame, as shown in Fig. 9. Further insight is provided by joint OH PLIF/LII images, as shown in Fig. 10. Low in the flame, soot begins to form near the OH layer on the edge of the flame. The flame has not entrained much air at these lower positions, so the soot is limited to a narrow range of radial positions, as seen in the LII data in Fig. 4. During those times that soot does make it to the centerline at these lower positions, it is due to an occasional strong interior vortex that pulls soot over from the flame front region and/or an occasional strong vortex outside the flame sheet that drives it inward. In either case, the soot on the centerline is fairly hot. As one moves up the flame, the flame itself widens and the concerted action of the turbulence within the fuel jet mixes the soot that had formed near the flame front throughout the fuel-rich core of the jet. This mixing action cools the soot and also gives the soot time to radiate energy away and cool in this manner. As most of the fuel becomes consumed, the flame front moves inward in large vortical motions that allow the OH layer to reach the centerline and to clip-off soot-filled regions of the remaining fuel pyrolysis products.

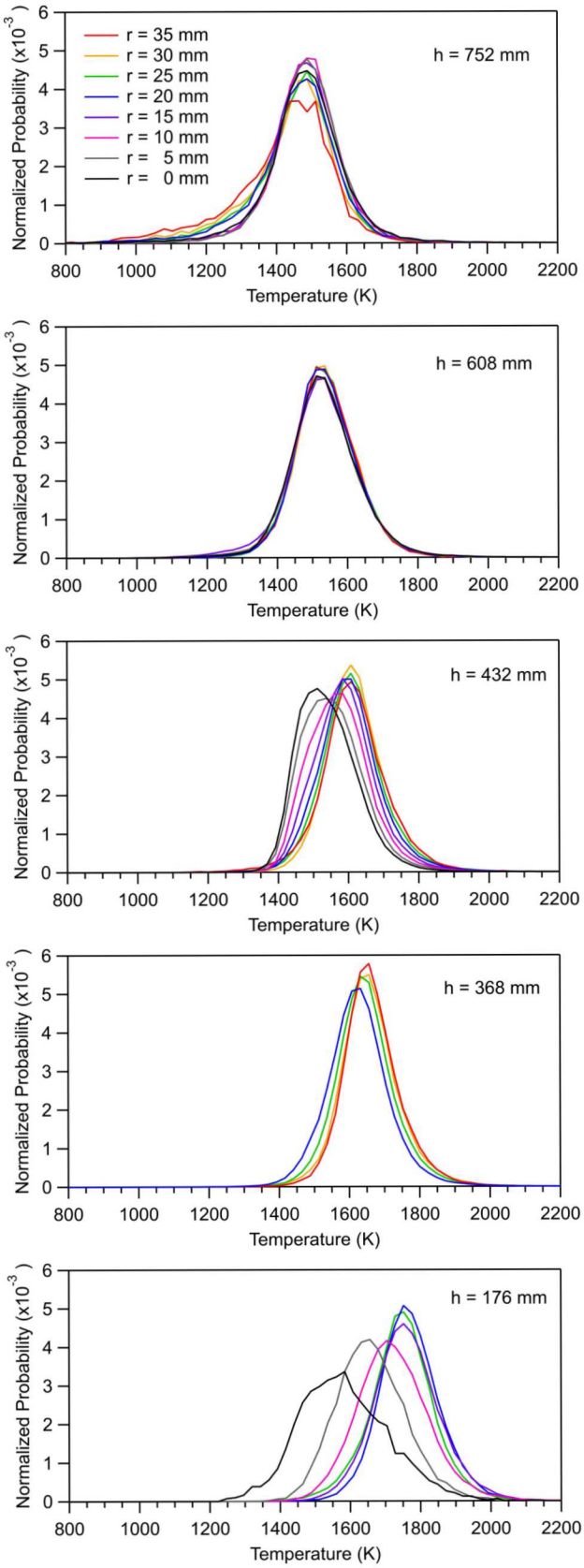

Figure 9: Normalized probability density functions of soot temperature as a function of radial position.

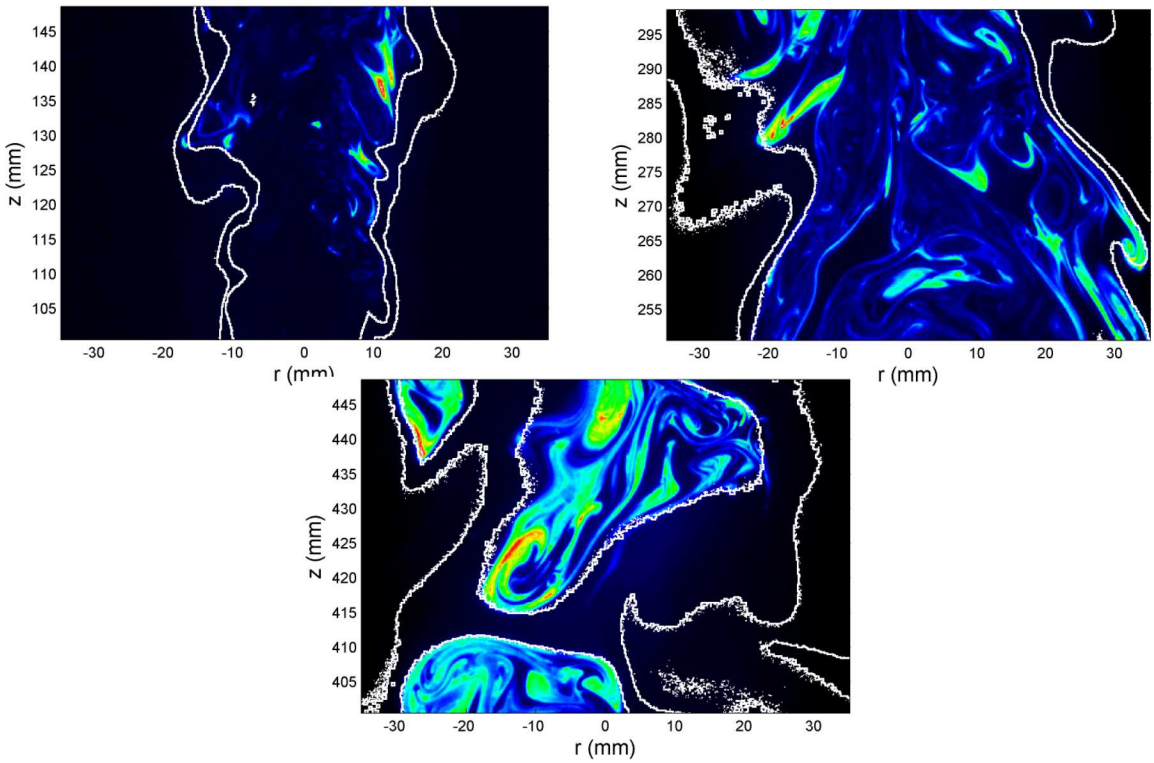

Figure 10. Overlay images of OH layer outlines (in white) on top of simultaneous LII images of soot concentration in the ethylene flame, at three different heights.

4. Conclusions

In this paper we present a full set of analyzed soot temperature data together with soot concentration and radiant emission data in a turbulent ethylene non-premixed jet flame burning in air. The time-averaged temperatures give perhaps a surprising trend of soot temperature peaking low in the flame, but an evaluation of previously collected simultaneous OH PLIF and soot LII images explains the flame physics behind the trends in the soot temperature data. This integrated set of measurements should comprise a challenging target for comparisons with turbulent flame models that include soot formation and radiant transport.

Acknowledgments

This work was primarily supported by the U.S. DoD's Strategic Environmental Research and Development Program (SERDP). Additional support in analyzing the data was provided through Sandia's Laboratory Directed Research and Development (LDRD) program. Sandia National Laboratories is a multimission laboratory managed and operated by National Technology and Engineering Solutions of Sandia, LLC., a wholly owned subsidiary of Honeywell International, Inc., for the U.S. Department of Energy's National Nuclear Security Administration under contract DE-NA-0003525. The views expressed in the article do not necessarily represent the views of the U.S. Department of Energy or the United States Government.

References

[1] R.D. Brook, S. Rajagopalan, C.A. Pope, J.R. Brook, A. Bhatnagar, A.V. Diez-Roux, F. Holguin, Y.L. Hong, R.V. Luepker, M.A. Mittleman, A. Peters, D. Siscovick, S.C. Smith, L. Whitsel, J.D. Kaufman, Particulate Matter Air Pollution and Cardiovascular Disease: An Update to the Scientific Statement From the American Heart Association, Circulation 121 (2010) 2331-2378.

[2] A.C. Rohr, R.E. Wyzga, Attributing health effects to individual particulate matter constituents, Atmos. Envir. 62 (2012) 130-152.

[3] A. Rohr, J. McDonald, Health effects of carbon-containing particulate matter: focus on sources and recent research program results, Crit. Rev. Toxic. 46 (2016) 97-137.

[4] J. Yang, P. Roth, C.R. Ruehl, M.M. Shafer, D.S. Antkiewicz, T.D. Durbin, D. Cocker, A. Asa-Awuka, G. Karavalakis, Physical, chemical, and toxicological characteristics of particulate emissions from current technology gasoline direct injection vehicles, Sci. Total Envir. 650 (2019) 1182-1194.

[5] R. Wang, Y. Balkanski, O. Boucher, P. Ciais, G.L. Schuster, F. Chevallier, B.H. Samset, J. Liu, S. Piao, M. Valari, S. Tao, Estimation of global black carbon direct radiative forcing and its uncertainty constrained by observations, J. Geophys. Res. Atmos. 121 (2016) 5948-5971.

[6] R. Watson, J. Houghton, D. Yihui, B. Metz, O. Davidson, N. Sundararaman, D. Griggs, D. Dokken, *Aviation and the Global Atmosphere*, a special report of the Intergovernmental Panel on Climate Change (IPCC), 1999, available from http://www.ipcc.ch/ipccreports/sres/aviation/index.htm

[7] R.S. Barlow, Laser diagnostics and their interplay with computations to understand turbulent combustion, Proc. Combust. Instit. 31 (2007) 49-75.

[8] N.H. Qamar, Z.T. Alwahabi, Q.N. Chan, G.J. Nathan, D. Roekaerts, K.D. King, Soot volume fraction in a piloted turbulent jet non-premixed flame of natural gas, Combust. Flame 156 (2009) 1339-1347.

[9] A. Gupta, D.C. Haworth, M.F. Modest, Turbulence-radiation interactions in large-eddy simulations of luminous and nonluminous nonpremixed flames, Proc. Combust. Instit. 34 (2013) 1281-1288.

[10] J. Zhang, C.R. Shaddix, R.W. Schefer, Design of "model-friendly" turbulent non-premixed jet burners for C_{2+} hydrocarbon fuels, Rev. Sci. Instr.82 (2011) 074101.

[11] A.R. Masri, R.W. Dibble, R.S. Barlow, The structure of turbulent nonpremixed flames revealed by Raman-Rayleigh-LIF measurements, Prog. Energy Combust. Sci. 22 (1996) 307-362.

[12] K. Gkagkas, R.P. Lindstedt, T.S. Kuan, Transported PDF Modelling of a High Velocity Bluff-Body Stabilised Flame (HM2) Using Detailed Chemistry, Flow Turb. Combust. 82 (2009) 493-509.

[13] R.L. Vander Wal, Laser-induced incandescence: detection issues, Appl. Optics 35 (1996) 6548-6548.

[14] F. Goulay, P.E. Schrader, L. Nemes, M.A. Dansson, H.A. Michelsen, Photochemical interferences for laser-induced incandescence of flame-generated soot, Proc. Combust. Instit. 32 (2009) 963-970.

[15] T.C. Williams, C.R. Shaddix, K.A. Jensen, J.M. Suo-Anttila, Measurement of the dimensionless extinction coefficient of soot within laminar diffusion flames, Int. J. Heat Mass Trans. 50 (2007) 1616-1630.

[16] C.R. Shaddix, K.C. Smyth, Laser-induced incandescence measurements of soot production in steady and flickering methane, propane, and ethylene diffusion flames, Combust. Flame 107 (1996) 418–452.

[17] F. Liu, K.A. Thomson, G.J. Smallwood, Numerical investigation of the effect of signal trapping on soot measurements using LII in laminar coflow diffusion flames, Appl. Phys. B 96 (2009) 671-682.

[18] T.C. Bond, R.H. Bergstrom, Light Absorption by Carbonaceous Particles: An Investigative Review, Aerosol Sci. Tech. 40 (2006) 27-67.

[19] Y.R. Sivathanu, G.M. Faeth, Temperature/Soot Volume Fraction Correlations in the Fuel-Rich Region of Buoyant Turbulent Diffusion Flames, Combust. Flame 81 (1990) 150-165.

[20] A. Coppalle, D. Joyeux, Temperature and Soot Volume Fraction in Turbulent Diffusion Flames: Measurements of Mean and Fluctuating Values, Combust. Flame 96 (1994) 275-285.

[21] B. Hu, B. Yang, U.O. Koylu, Soot measurements at the axis of an ethylene/air non-premixed turbulent jet flame, Combust. Flame 134 (2003) 93-106.

[22] S.-Y. Lee, S.R. Turns, R.J. Santoro, Measurements of soot, OH, and PAH concentrations in turbulent ethylene/air jet flames, Combust. Flame 156 (2009) 2264-2275.